Chapter 14

TELEPORTATION THROUGH THE WORMHOLE

This chapter includes the work published as:

[1] Daniel Jafferis, Alexander Zlokapa, Joseph D. Lykken, David K. Kolchmeyer, Samantha I. Davis, Nikolai Lauk, Hartmut Neven, and Maria Spiropulu. "Traversable wormhole dynamics on a quantum processor." In: Nature 612.7938 (2022), pp. 51–55.

14.1 Introduction

Traversable wormholes [1, 2] provide a mechanism to probe the conjectured ER=EPR relation between entanglement and spacetime geometry [3, 4] via the holographic correspondence of quantum many-body systems and gravitational physics [5]. In this construction, a pair of black holes in a thermofield double state have their interiors connected via an Einstein-Rosen bridge. Classically, the null energy condition prevents such wormholes from being traversable [6, 7, 8, 9]. The basic mechanism found in Ref. [1] is that the gravitational backreaction to quantum effects induced by couplings between the exterior regions of the pair of black holes can render the wormhole traversable [10]. It was demonstrated by Refs. [1, 2] that sending quantum information through such a wormhole is the gravitational description of quantum teleportation in the dual many-body system: the physical picture behind this teleportation is that the qubit traverses the emergent wormhole.

Considering gravity with nearly AdS_2 boundary conditions [11], the thermofield double (TFD) state corresponds to an AdS-Schwarzschild wormhole [12]. Two quantum systems — denoted L and R for the two black holes — are entangled in the TFD state at temperature $1/\beta$. In the gravitational picture, a qubit is injected into L at time $-t_0$ and arrives at R at t_1 due to a coupling interaction at $t = 0$. This coupling induces a negative null energy in the bulk that shifts the qubit away from the singularity (Fig. 14.1a), consistent with a quantum computation that recovers the infalling qubit under unitary black hole dynamics [13]. Interpreted in terms of recovering information from unitary black hole evaporation [13], the negative energy shockwave produces a quantum computation that causes the scrambled infalling qubit to reappear in the auxiliary entangled system, i.e., emerging at R after a

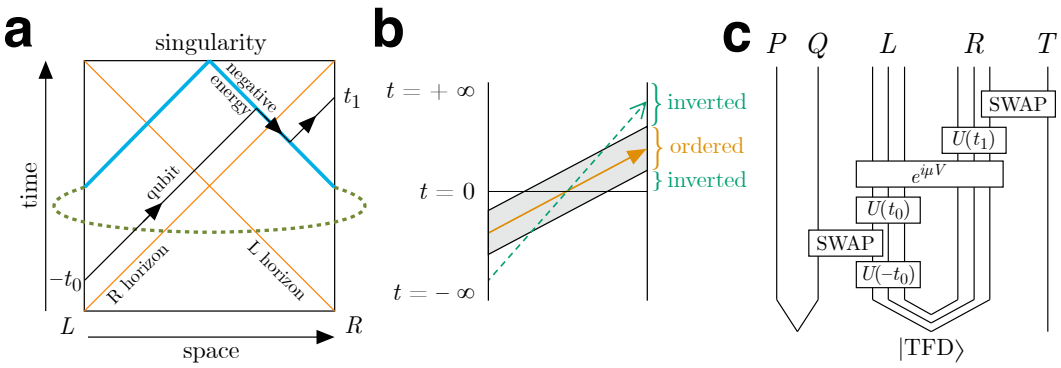

Figure 14.1: Traversable wormhole in spacetime and in the holographic dual. a) Diagram of a traversable wormhole in anti-de Sitter space. A qubit injected at $t = -t_0$ enters through the left side of the wormhole; at $t = 0$ a coupling (dashed line) is applied between the two sides of the wormhole, causing a negative energy shockwave (blue); the qubit experiences a time advance upon contact with the shockwave, causing it to emerge from the right side at $t = t_1$. b) Illustration of time-ordering (wormhole) and time-inversion (scrambling) of teleportation signals. The smooth semiclassical geometry of a traversable wormhole produces a regime of teleportation that obeys causality; non-gravitational teleportation causes the signals to arrive in reverse order. c) The traversable wormhole expressed as a quantum circuit, equivalent to the gravitational picture in the semiclassical limit of an infinite number of qubits. The unitary $\hat{U}(t)$ denotes time evolution $e^{-i(\hat{H}_L+\hat{H}_R)t}$ under the left and right SYK models. The thermofield double state ($|\mathrm{TFD}\rangle$) initializes the wormhole at $t = 0$. The time evolution and Majorana fermion SWAP gates achieve qubit injection and arrival readout at the appropriate times. When $\mu < 0$, the coupling $e^{i\mu\hat{V}}$ generates a negative energy shockwave, allowing traversability; when $\mu > 0$, the coupling generates a positive energy shockwave and the qubit falls into the singularity.

time of order the scrambling time. If the sign of the interaction is reversed, the qubit irretrievably falls into the singularity. Wormhole teleportation corresponds to on-shell propagation through the bulk from the left to the right boundary. The time-ordering of the transmitted quantum information is then preserved through the wormhole (Fig. 14.1b), unlike teleportation by random unitary dynamics [14, 15, 16, 17, 18].

In the semiclassical limit of an infinite number of qubits, it is known that the SYK model [19, 20] may be used to experimentally realize traversable wormhole dynamics [21]. In this work, we study the dynamics of traversable wormholes via many-body simulation of an SYK-like system of N fermions [19, 20], where traversable wormhole protocol is equivalent to a quantum teleportation protocol in the large-N semiclassical limit (Fig. 14.1c).

14.2 Traversable wormhole teleportation protocol

To implement the quantum teleportation protocol, we initialize the thermofield double state $|\text{TFD}\rangle = \frac{1}{\sqrt{Z}} \sum_n e^{-\beta E_n/2} |n\rangle_L \otimes |n\rangle_R$, where $|n\rangle_{L,R}$ are the energy eigenstates of the left and right SYK systems. Explicitly, given left and right Hamiltonians $\hat{H}_L$ and $\hat{H}_R$ with N Majorana fermions $\hat{\psi}$ on each side, the SYK model with q couplings is given by

$$\hat{H}_{L,R} = \sum_{1 \le j_1 < \cdots < j_q \le N} J_{j_1 \ldots j_q} \hat{\psi}^{j_1}_{L,R} \ldots \hat{\psi}^{j_q}_{L,R}, \tag{14.1}$$

where the couplings are chosen from a Gaussian distribution with mean zero and variance $J^2(q-1)!/N^{q-1}$. To swap in a qubit at $t = -t_0$, the system is time-evolved by $e^{-i\hat{H}t}$ for $\hat{H} \equiv \hat{H}_L + \hat{H}_R$. At $t = 0$, the interaction $e^{i\mu\hat{V}}$ is applied across both the left and right subsystems with coupling operator $\hat{V} = \frac{1}{qN} \sum_j \hat{\psi}^j_L \hat{\psi}^j_R$. The sign of μ must be negative to produce a negative energy shockwave that allows the qubit to travel through the wormhole. We measure the mutual information I_{PT} given by

$$I_{PT}(t) = S_P(t) + S_T(t) - S_{PT}(t), \tag{14.2}$$

where S is a measure of entropy. If a quantum system were to teleport via scrambling rather than traversing a wormhole, the mutual information would be symmetric in μ. Perfect teleportation is achieved when I_{PT} is maximal. No information is transmitted when I_{PT} is zero.

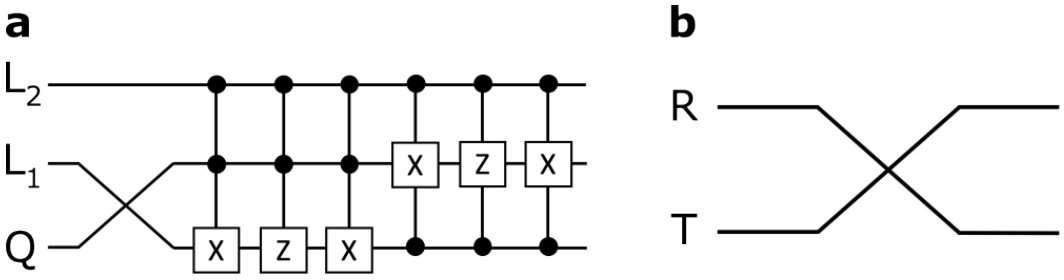

Figure 14.2: Majorana SWAP gates. a) $ZX + iZY$ Majorana SWAP gate decomposition for inserting a qubit (Q) into the wormhole. L_1, L_2 are qubits in the left subsystem. b) $X + iY$ Majorana SWAP gate for extracting the qubit from the wormhole, which coincidences with the regular SWAP gate. R is a qubit in the right subsystem and T is the register.

14.3 Experimental implementation

To implement the wormhole protocol experimentally, the protocol needs to be decomposed into a quantum circuit that can be realized on near-term quantum hardware. We consider a system of $2N$ Majorana fermions, with N Majorana fermions on each of the left and right subsystems, corresponding to a total of N qubits. Each Majorana fermion in the Hamiltonian is encoded in a digital quantum processor via the standard Jordan-Wigner transformation to Pauli strings. Specifically, Majorana fermions are transformed to the form $\frac{1}{\sqrt{2}}Z^{\otimes k}X$ or $\frac{1}{\sqrt{2}}Z^{\otimes k}Y$ for $k \in [1, N]$. The choice of the mapping between each $\hat{\psi}^i_{L,R}$ and each Pauli string is optimized to minimize the required number of two-qubit gates to perform the wormhole teleportation protocol. We choose the Jordan-Wigner transformation as follows, where Z^i indicates $Z \otimes \cdots \otimes Z$,

$$\begin{aligned}
\hat{\psi}^1_L &= \tfrac{1}{\sqrt{2}}ZX, \quad \hat{\psi}^1_R = \tfrac{1}{\sqrt{2}}X, \\
\hat{\psi}^2_L &= \tfrac{1}{\sqrt{2}}ZY, \quad \hat{\psi}^2_R = \tfrac{1}{\sqrt{2}}Y, \\
\hat{\psi}^3_L &= \tfrac{1}{\sqrt{2}}Z^5X, \quad \hat{\psi}^3_R = \tfrac{1}{\sqrt{2}}Z^5Y, \\
\hat{\psi}^4_L &= \tfrac{1}{\sqrt{2}}Z^2X, \quad \hat{\psi}^4_R = \tfrac{1}{\sqrt{2}}Z^2Y, \\
\hat{\psi}^5_L &= \tfrac{1}{\sqrt{2}}Z^4X, \quad \hat{\psi}^5_R = \tfrac{1}{\sqrt{2}}Z^4Y, \\
\hat{\psi}^6_L &= \tfrac{1}{\sqrt{2}}Z^3X, \quad \hat{\psi}^6_R = \tfrac{1}{\sqrt{2}}Z^3Y, \\
\hat{\psi}^7_L &= \tfrac{1}{\sqrt{2}}Z^6X, \quad \hat{\psi}^7_R = \tfrac{1}{\sqrt{2}}Z^6Y.
\end{aligned} \tag{14.3}$$

The particular choice of $\hat{\psi}^1_R = \frac{1}{\sqrt{2}}X$, $\hat{\psi}^2_R = \frac{1}{\sqrt{2}}Y$, $\hat{\psi}^1_L = \frac{1}{\sqrt{2}}ZX$, $\hat{\psi}^2_L = \frac{1}{\sqrt{2}}ZY$ ensures that the decomposition of Majorana SWAP gates into two-qubit gates is efficient.

To swap a qubit into or out of the wormhole, we pair up Majorana fermions on a single qubit into a Dirac fermion $\hat{\chi} = \frac{1}{2}(Z^{\otimes k}X + iZ^{\otimes k}Y)$. The appropriate SWAP operator is given by,

$$\text{SWAP} = \begin{bmatrix} \hat{\chi}\hat{\chi}^\dagger & \hat{\chi}^\dagger \\ \hat{\chi} & \hat{\chi}^\dagger\hat{\chi} \end{bmatrix}. \tag{14.4}$$

To reduce the number of two-qubit gates, we restrict our attention to Jordan-Wigner transforms that only swap into or out of $X + iY$ and $ZX + iZY$. Explicitly, the SWAP operators for extracting a qubit from and inserting a qubit into the system, respectively, are given by,

$$\text{SWAP}_{X+iY} = \begin{bmatrix} 1 & 0 & 0 & 0 \\ 0 & 0 & 1 & 0 \\ 0 & 1 & 0 & 0 \\ 0 & 0 & 0 & 1 \end{bmatrix}, \tag{14.5}$$

$$\text{SWAP}_{ZX+iZY} = \begin{bmatrix} 1 & 0 & 0 & 0 & 0 & 0 & 0 & 0 \\ 0 & 0 & 1 & 0 & 0 & 0 & 0 & 0 \\ 0 & 1 & 0 & 0 & 0 & 0 & 0 & 0 \\ 0 & 0 & 0 & 1 & 0 & 0 & 0 & 0 \\ 0 & 0 & 0 & 0 & 1 & 0 & 0 & 0 \\ 0 & 0 & 0 & 0 & 0 & 0 & -1 & 0 \\ 0 & 0 & 0 & 0 & 0 & -1 & 0 & 0 \\ 0 & 0 & 0 & 0 & 0 & 0 & 0 & 1 \end{bmatrix}. \tag{14.6}$$

The gate decomposition of the swap operators is shown in Fig. 14.2. Since the $X+iY$ Majorana SWAP coincides with the standard SWAP given by Eq. 14.5, the final SWAP in the protocol from R to T (Fig. 14.1c) is replaced by direct measurement of the rightmost qubit of R to further reduce gate count. The $ZX + iZY$ SWAP operator for the initial SWAP of the protocol is decomposed into gates using the prescription in Ref. [22], which recursively decomposes an arbitrary unitary matrix into a product of fully-controlled quantum gates.

We proceed to the decomposition of the time evolution operator, $\hat{U}(t) = e^{-i(\hat{H}_L+\hat{H}_R)t}$, for the SYK model. We choose $q = 4$ and perform numerical simulations to identify sufficiently small N that could be experimentally implemented while preserving features of the gravitational physics. Our numerical simulation shows that $N = 10$ is sufficient to produce such traversable wormhole behavior (Fig. 14.3). When $\mu < 0$, mutual information is expected to peak around the scrambling time in the limit of

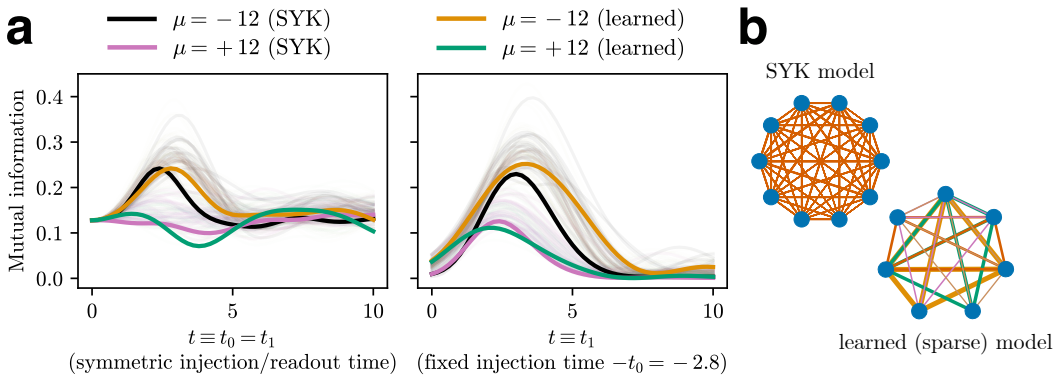

Figure 14.3: Learning a traversable wormhole Hamiltonian from the SYK model. a) Mutual information of multiple $N = 10$ SYK models (black and purple, $\beta = 4$) and corresponding learned Hamiltonians (orange and green) showing asymmetry in coupling with $\mu < 0$ (wormhole teleportation) and $\mu > 0$ (scrambling teleportation). Thick lines show a specific instantiation of an SYK model and its corresponding learned sparsification with 5 nonzero coefficients (Eq. 14.7); light lines indicate a population of SYK models and learned sparsifications with 5 to 10 nonzero coefficients, demonstrating the reliability of the learning procedure. The learned Hamiltonian is trained only on the mutual information $I_{PT}(t)$ for $t \equiv t_0 = t_1$ (left), and its behavior is consistent with the a wormhole after a qubit is injected at fixed $-t_0$ (right). b) Sparsification of the original SYK model with 210 nonzero coefficients (top) to the learned Hamiltonian with 5 nonzero coefficients (bottom, Eq. 14.7). Groups of four Majorana fermions (blue dots) are coupled with coefficients. Line thickness indicates coefficient magnitude, and color distinguishes individual coefficients (bottom only).

large N. The peaking behavior of $I_{PT}(t)$ may be observed in two ways: either by setting the injection and readout times to be symmetric ($t \equiv t_0 = t_1$), or by fixing the time of injection (fixed t_0) and measuring different readout times ($t \equiv t_1$). In the semiclassical gravity description, a pole in the causal left-right propagator corresponds to timelike geodesics connecting the left and right systems — i.e., a traversable wormhole in the bulk geometry [2]. Hence, we expect the teleportation signal to be maximized when $t_0 \approx t_1 \approx t_*$ for scrambling time t_*. We measure the corresponding peak signature in $I_{PT}(t)$ for both $t \equiv t_0 = t_1$ and $t \equiv t_1$ (fixed t_0). This result is reinforced by a theoretical analysis of chord diagrams in the double-scaled limit [23] and comparison to prior numerical results [24, 25, 26] (see Supplementary Information of Ref. [27]).

Nevertheless, the circuit depth $\sim O(N^4)$ to experimentally implement an $N = 10$ SYK system remains prohibitive on current hardware. We turn to sparsification of the SYK system and produce evidence of gravitational physics in the sparsified system. Sparsification of the SYK system (i.e., setting many $J_{j_1 \ldots j_4}$ to zero) is shown to preserve gravitational physics even when the number of terms in the Hamiltonian is randomly reduced from $O(N^4)$ to kN with k of order unity [28, 29, 30]. Here, we apply techniques from machine learning to optimize the sparsification procedure. The result reduces an $N = 10$ SYK model with 210 terms to an $N = 7$ model with 5 terms, yielding a 9-qubit circuit for the wormhole teleportation protocol. While larger Hamiltonians may provide a stronger teleportation signal, additional gates at current hardware fidelity further attenuate the signal (see Supplementary Information of Ref. [27]); hence, we restrict our attention to the smallest sparsified model with gravitational properties and do not enter the beyond-classical regime.

We construct an analogue of training a neural network. Due to unitarity and differentiability of the quantum circuit, backpropagation across the wormhole teleportation protocol allows gradient descent to optimize the $J_{j_1 \ldots j_4}$ coefficients with regularization, interpreting the Hamiltonian coefficients as neural network weights. The dataset consists of $I_{PT}(t)$ with $t \equiv t_0 = t_1$ for a standard wormhole constructed by the SYK model with Gaussian-distributed coefficients. The loss function is chosen to be the total mean squared error of $I_{PT}(t)$ for both positive and negative values of a fixed interaction coupling μ, where μ is chosen to maximize the mutual information. Training with weight regularization and truncation sparsifies the Hamiltonian while preserving mutual information dynamics.

Applying the learning process, we produce a large population of sparse Hamiltonians exhibiting the appropriate interaction sign dependence (Fig. 14.3a). We select the Hamiltonian,

$$\begin{aligned} \hat{H}_{L,R} = &- 0.36\hat{\psi}^1\hat{\psi}^2\hat{\psi}^4\hat{\psi}^5 + 0.19\hat{\psi}^1\hat{\psi}^3\hat{\psi}^4\hat{\psi}^7 \\ &- 0.71\hat{\psi}^1\hat{\psi}^3\hat{\psi}^5\hat{\psi}^6 + 0.22\hat{\psi}^2\hat{\psi}^3\hat{\psi}^4\hat{\psi}^6 \\ &+ 0.49\hat{\psi}^2\hat{\psi}^3\hat{\psi}^5\hat{\psi}^7, \end{aligned} \tag{14.7}$$

which requires 7 of the original $N = 10$ SYK model fermions, where $\hat{\psi}^j$ denotes the Majorana fermions of either the left or the right systems. Investigation of the sparse learned Hamiltonian in Eq. 14.7 and its description of gravitational physics are in Appendix F. We find that the Hamiltonian is consistent with gravitational dynamics of the dense SYK Hamiltonian beyond its training data and satisfies necessary

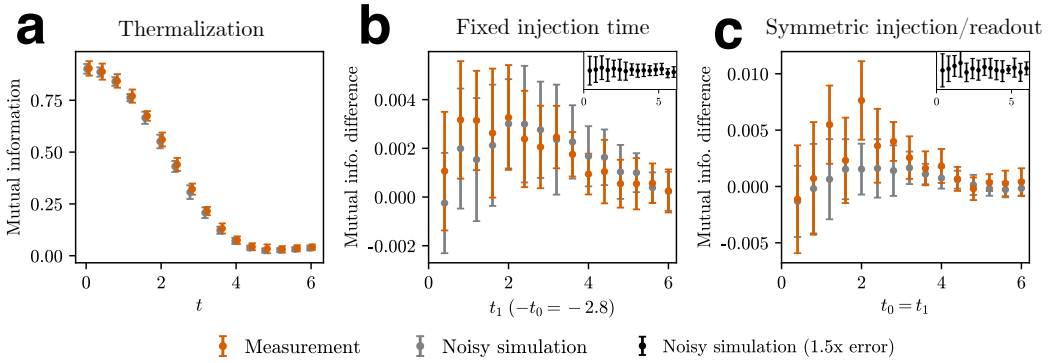

Figure 14.4: Observation of traversable wormhole dynamics. a) Thermalization protocol (109 CZ gates), measuring the mutual information between a qubit injected into a sparse SYK model at time $-t$ and at t. Error bars show three standard deviations over 20 runs. b) Traversable wormhole with fixed injection time (164 CZ gates), showing the difference in mutual information between $\mu = -12$ and $\mu = +12$. Error bars show one standard deviation over 28 runs. c) Traversable wormhole with symmetric injection and readout time (164 CZ gates), showing the difference in mutual information between $\mu = -12$ and $\mu = +12$. Error bars show one standard deviation over 20 runs. Insets show noisy simulations with gate errors increased by a factor of 1.5, plotted with y-axis mutual information range $[-3 \times 10^{-3}, 3 \times 10^{-3}]$; the peak is not visible. The measurements in b) and c) agree with noisy simulation and reproduce the sign asymmetry of the mutual information consistent with through-the-wormhole teleportation. The scrambling-unscrambling dynamics of wormhole teleportation cause the mutual information to be significantly attenuated by noise. In noisy simulations, each gate is subjected to depolarization error determined by calibration data (median CZ error: 0.3%). Each run consists of 90,000 measurements.

criteria of general holographic systems: perfect size winding, Shapiro time delay, and causally time-ordered teleportation [31, 32, 18].

We initialize the protocol of Fig. 14.1c by preparing the TFD state using a hardware-efficient variational quantum eigensolver [33] as the ground state of the Hamiltonian $\hat{H}_{\text{TFD}} = \hat{H}_L + \hat{H}_R + i\nu\hat{V}$ where $\hat{V}$ is the usual coupling operator. The ground state of $\hat{H}_{\text{TFD}}$ is approximately the thermofield double state with inverse temperature $O(1/\nu)$ [34, 35]. Time evolution and the interaction $e^{i\mu\hat{V}}$ are applied with a single Trotter step. This is sufficient to achieve a close approximation for the relevant range of t, i.e., the number of gates remains constant for all times.

14.4 Traversable wormhole dynamics on a quantum processor

Here, we proceed with a quantum experiment. Namely, we realize the entangled system on the Google Sycamore superconducting qubit array [36] with a 9-qubit circuit of 164 controlled-Z gates and 295 single-qubit gates. A noisy simulation assuming all gate errors are depolarizing noise agrees with the experimental measurement of the quantum system as shown in Fig. 14.4. A simpler protocol measuring thermalization with 109 CZ gates (Fig. 14.4a) demonstrates the high fidelity of the experiment; additional experiments with $\mu = 0$ confirm that coherent errors are dominated by the true teleportation signal (see Supplementary Information of Ref. [27]). Measuring the traversable wormhole protocol (Fig. 14.4b, c), we observe increased teleportation when the interaction introduces a negative energy shockwave rather than a positive one. The asymmetric signature is consistent with the physical interpretation that the qubit underwent teleportation through the wormhole. The scrambling-unscrambling dynamics of wormhole teleportation is sensitive to errors: at gate error rates larger than our experiment by a factor of 1.5, the asymmetric wormhole peak-like signal cannot be resolved (see Fig. 14.4 insets).

We find that the protocol is efficiently scalable to larger system sizes. To satisfy limitations of current quantum hardware, we adopted techniques from machine learning to construct a small-N sparse Hamiltonian that preserves gravitational physics. For systems with $N = O(50)$ fermions, random sparsification is as effective as optimal sparsification up to an order unity constant [28, 29, 30]. This removes the need for classical simulation without introducing significant overhead, successfully extending to the beyond-classical regime.

This work is the first successful attempt to investigate traversable wormhole dynamics in an experimental setting. Looking forward, we anticipate that near-term quantum computers that extend beyond the capabilities of classical simulation will coincide with system sizes that provide novel gravitational insight. At too large N, semiclassical gravity describes system dynamics; at too small N, relevant features may not be resolvable. In the regime of $N = O(100)$ fermions, measurement of inelastic effects in the bulk may provide quantitative insights into aspects of quantum gravity that are poorly understood from a theoretical perspective, such as string production and finite-N corrections to scattering. We conclude that the demonstrated approach of on-chip quantum experimentation of gravity promises future insights into the holographic correspondence.

References

[1] Ping Gao, Daniel Louis Jafferis, and Aron C Wall. "Traversable wormholes via a double trace deformation." In: Journal of High Energy Physics 2017.12 (2017), p. 151.

[2] Juan Maldacena, Douglas Stanford, and Zhenbin Yang. "Diving into traversable wormholes." In: Fortschritte der Physik 65.5 (2017), p. 1700034.

[3] J. Maldacena and L. Susskind. "Cool horizons for entangled black holes." In: Fortschritte der Physik 61.9 (2013), pp. 781–811. DOI: https://doi.org/10.1002/prop.201300020.

[4] Leonard Susskind. Dear Qubitzers, GR=QM. 2017. arXiv: 1708.03040 [hep-th].

[5] Juan Maldacena. "The large-N limit of superconformal field theories and supergravity." In: International journal of theoretical physics 38.4 (1999), pp. 1113–1133.

[6] David Hochberg and Matt Visser. "The Null energy condition in dynamic wormholes." In: Physical Review Letters 81 (1998), pp. 746–749. DOI: 10.1103/PhysRevLett.81.746. arXiv: gr-qc/9802048.

[7] M. S. Morris, K. S. Thorne, and U. Yurtsever. "Wormholes, Time Machines, and the Weak Energy Condition." In: Physical Review Letters 61 (1988), pp. 1446–1449. DOI: 10.1103/PhysRevLett.61.1446.

[8] Matt Visser, Sayan Kar, and Naresh Dadhich. "Traversable wormholes with arbitrarily small energy condition violations." In: Physical Review Letters 90 (2003), p. 201102. DOI: 10.1103/PhysRevLett.90.201102. arXiv: gr-qc/0301003.

[9] M. Visser. Lorentzian Wormholes: From Einstein to Hawking. Computational and Mathematical Physics. American Inst. of Physics, 1995. ISBN: 9781563963940.

[10] Noah Graham and Ken D. Olum. "Achronal averaged null energy condition." In: Physical Review D 76 (2007), p. 064001. DOI: 10.1103/PhysRevD.76.064001. arXiv: 0705.3193 [gr-qc].

[11] Juan Maldacena, Douglas Stanford, and Zhenbin Yang. "Conformal symmetry and its breaking in two dimensional Nearly Anti-de-Sitter space." In: PTEP 2016.12 (2016), p. 12C104. DOI: 10.1093/ptep/ptw124. arXiv: 1606.01857 [hep-th].

[12] Juan Maldacena. "Eternal black holes in anti-de Sitter." In: Journal of High Energy Physics 2003.04 (Apr. 2003), pp. 021–021. DOI: 10.1088/1126-6708/2003/04/021. URL: https://doi.org/10.1088/1126-6708/2003/04/021.

[13] Patrick Hayden and John Preskill. "Black holes as mirrors: quantum information in random subsystems." In: Journal of high energy physics 2007.09 (2007), p. 120.

[14] Leonard Susskind and Ying Zhao. "Teleportation through the wormhole." In: Physical Review D 98 (4 Aug. 2018), p. 046016. DOI: 10.1103/PhysRevD.98.046016. URL: https://link.aps.org/doi/10.1103/PhysRevD.98.046016.

[15] Ping Gao and Hong Liu. "Regenesis and quantum traversable wormholes." In: JHEP 10 (2019), p. 048. DOI: 10.1007/JHEP10(2019)048. arXiv: 1810.01444 [hep-th].

[16] Beni Yoshida and Norman Y. Yao. "Disentangling Scrambling and Decoherence via Quantum Teleportation." In: Physical Review X 9 (1 Jan. 2019), p. 011006. DOI: 10.1103/PhysRevX.9.011006. URL: https://link.aps.org/doi/10.1103/PhysRevX.9.011006.

[17] Kevin A. Landsman, Caroline Figgatt, Thomas Schuster, Norbert M. Linke, Beni Yoshida, Norm Y. Yao, and Christopher Monroe. "Verified quantum information scrambling." In: Nature 567.7746 (2019), pp. 61–65.

[18] Thomas Schuster, Bryce Kobrin, Ping Gao, Iris Cong, Emil T Khabiboulline, Norbert M Linke, Mikhail D Lukin, Christopher Monroe, Beni Yoshida, and Norman Y Yao. "Many-body quantum teleportation via operator spreading in the traversable wormhole protocol." In: Physical Review X 12.3 (2022), p. 031013.

[19] Subir Sachdev and Jinwu Ye. "Gapless spin-fluid ground state in a random quantum Heisenberg magnet." In: Physical Review Letters 70 (21 May 1993), pp. 3339–3342. DOI: 10.1103/PhysRevLett.70.3339. URL: https://link.aps.org/doi/10.1103/PhysRevLett.70.3339.

[20] Alexei Kitaev. "A simple model of quantum holography." In: KITP strings seminar and Entanglement. Vol. 12. 2015, p. 26.

[21] Ping Gao and Daniel Louis Jafferis. "A traversable wormhole teleportation protocol in the SYK model." In: Journal of High Energy Physics 2021.7 (2021), pp. 1–44.

[22] Chi-Kwong Li and Diane Pelejo. Decomposition of quantum gates. 2013. arXiv: 1311.3599 [quant-ph].

[23] Micha Berkooz, Mikhail Isachenkov, Vladimir Narovlansky, and Genis Torrents. "Towards a full solution of the large N double-scaled SYK model." In: JHEP 03 (2019), p. 079. DOI: 10.1007/JHEP03(2019)079. arXiv: 1811.02584 [hep-th].

[24] Jordan S. Cotler, Guy Gur-Ari, Masanori Hanada, Joseph Polchinski, Phil Saad, Stephen H. Shenker, Douglas Stanford, Alexandre Streicher, and Masaki Tezuka. "Black holes and random matrices." In: Journal of High Energy Physics 2017.5 (May 2017), p. 118. ISSN: 1029-8479. DOI: 10.1007/JHEP05(2017)118. URL: https://doi.org/10.1007/JHEP05(2017)118.

[25] Antonio M. García-García and Jacobus J. M. Verbaarschot. "Spectral and thermodynamic properties of the Sachdev-Ye-Kitaev model." In: Physical Review D 94 (12 2016), p. 126010. DOI: 10.1103/PhysRevD.94.126010. URL: https://link.aps.org/doi/10.1103/PhysRevD.94.126010.

[26] Antonio M. García-García and Jacobus J. M. Verbaarschot. "Analytical spectral density of the Sachdev-Ye-Kitaev model at finite N." In: Physical Review D 96 (6 Sept. 2017), p. 066012. DOI: 10.1103/PhysRevD.96.066012. URL: https://link.aps.org/doi/10.1103/PhysRevD.96.066012.

[27] Daniel Jafferis, Alexander Zlokapa, Joseph D. Lykken, David K. Kolchmeyer, Samantha I. Davis, Nikolai Lauk, Hartmut Neven, and Maria Spiropulu. "Traversable wormhole dynamics on a quantum processor." In: Nature 612.7938 (2022), pp. 51–55.

[28] Shenglong Xu, Leonard Susskind, Yuan Su, and Brian Swingle. A Sparse Model of Quantum Holography. 2020. arXiv: 2008.02303 [cond-mat.str-el].

[29] Antonio M. Garcia-Garcia, Yiyang Jia, Dario Rosa, and Jacobus J. M. Verbaarschot. "Sparse Sachdev-Ye-Kitaev model, quantum chaos, and gravity duals." In: Physical Review D 103 (10 2021), p. 106002. DOI: 10.1103/PhysRevD.103.106002. URL: https://link.aps.org/doi/10.1103/PhysRevD.103.106002.

[30] Elena Caceres, Anderson Misobuchi, and Rafael Pimentel. "Sparse SYK and traversable wormholes." In: JHEP 11 (2021), p. 015. DOI: 10.1007/JHEP11(2021)015. arXiv: 2108.08808 [hep-th].

[31] Adam R. Brown, Hrant Gharibyan, Stefan Leichenauer, Henry W. Lin, Sepehr Nezami, Grant Salton, Leonard Susskind, Brian Swingle, and Michael Walter. Quantum Gravity in the Lab: Teleportation by Size and Traversable Wormholes. 2021. arXiv: 1911.06314 [quant-ph].

[32] Sepehr Nezami, Henry W. Lin, Adam R. Brown, Hrant Gharibyan, Stefan Leichenauer, Grant Salton, Leonard Susskind, Brian Swingle, and Michael Walter. Quantum Gravity in the Lab: Teleportation by Size and Traversable Wormholes, Part II. 2021. arXiv: 2102.01064 [quant-ph].

[33] Abhinav Kandala, Antonio Mezzacapo, Kristan Temme, Maika Takita, Markus Brink, Jerry M Chow, and Jay M Gambetta. "Hardware-efficient variational quantum eigensolver for small molecules and quantum magnets." In: Nature 549.7671 (2017), pp. 242–246.

[34] Juan Maldacena and Xiao-Liang Qi. Eternal traversable wormhole. 2018. arXiv: 1804.00491 [hep-th].

[35] William Cottrell, Ben Freivogel, Diego M Hofman, and Sagar F Lokhande. "How to build the thermofield double state." In: Journal of High Energy Physics 2019.2 (2019), p. 58.

[36] Frank Arute, Kunal Arya, Ryan Babbush, et al. "Quantum supremacy using a programmable superconducting processor." In: Nature 574.7779 (Oct. 2019), pp. 505–510. ISSN: 1476-4687. DOI: 10.1038/s41586-019-1666-5. URL: https://doi.org/10.1038/s41586-019-1666-5.